2004

Analytical Solution for the Impedance of a Porous Electrode

Sheba Devan

Venkat R. Subramanian
University of South Carolina - Columbia

Ralph E. White
University of South Carolina - Columbia, white@cec.sc.edu

Publication Info

Published in *Journal of the Electrochemical Society*, Volume 151, Issue 6, 2004, pages A905-A913.

Devan, S., Subramanian, V.R., & White, R.E. (2004). Analytical Solution for the Impedance of a Porous Electrode. *Journal of the Electrochemical Society*, *151*(6): A905-A913.
Publisher's Version: http://dx.doi.org/10.1149/1.1739218

Journal of The Electrochemical Society, **151** (6) A905-A913 (2004)
0013-4651/2004/151(6)/A905/9/$7.00 © The Electrochemical Society, Inc.

Analytical Solution for the Impedance of a Porous Electrode

Sheba Devan,[a,*] Venkat R. Subramanian[b,] and R. E. White[a,***,z]**

[a]*Center for Electrochemical Engineering, Department of Chemical Engineering, Swearingen Engineering Center, University of South Carolina, Columbia, South Carolina 29208, USA*
[b]*Department of Chemical Engineering, Tennessee Technical University, Cookeville, Tennessee 38505, USA*

A macrohomogeneous model is presented for a porous electrode that includes coupled potential and concentration gradients with linear kinetics. The equations are solved to obtain an analytical expression for the impedance of a porous electrode. Complex plane plots are presented that illustrate two well-defined arcs: a kinetic arc and a diffusion arc with their time constants far apart. The effects of parameters such as exchange current density, porosity, diffusion coefficient, thickness, and interfacial area on the impedance spectra are presented. The usefulness of the analytical solution in investigating the effect of solution phase diffusion is also presented.
 [DOI: 10.1149/1.1739218]

Manuscript submitted June 24, 2003; revised manuscript received November 9, 2003. Available electronically May 4, 2004.

Electrochemical impedance spectroscopy (EIS) is a useful tool for studying porous electrodes, which are extensively used in the field of batteries, fuel cells, and electrochemical capacitors. The dynamics of the porous electrodes are governed by electrode kinetics at the solid/liquid interface, mass transfer in the solution phase, and conduction in both solution and matrix phases. The conductivities, specified by the type of matrix material and the electrolyte used, influence the potential distribution and concentration distribution across the electrode. The driving force for the electrode kinetics is the difference between the solution phase potential and the solid phase potential. Depending on the operating conditions, electrode kinetics, mass transfer, or both (mixed control) can control the transient behavior of the porous electrode. When the porous electrode is under mixed control both potential gradient and concentration gradients should be taken into account in modeling the impedance.

Mathematical models can be used to include both potential and concentration gradients. The work of de Levie[1] marks the start of many papers on the theory of the impedance of porous electrodes derived from various mathematical models. Two of the models are the cylindrical pore model and the macrohomogeneous model. The cylindrical pore model is based on the assumption that the porous electrode is composed of cylindrical pores of definite length and thickness, flooded with electrolyte. Using this theory, Lasia[2] developed equations for the impedance of a porous electrode under the influence of a potential gradient. Also Keddam *et al.*[3] developed an analytical solution for electrodes with concentration gradients only, neglecting the potential gradients. In the case of coupled gradients of potential and concentration for the cylindrical pore model, the impedance response has been determined numerically[4,5] and analytically.[6] Rangarajan[6] presented the analytical solution for the cylindrical pore model using dilute solution theory and discussed some of the limiting cases of his solution. He indicated that under certain conditions the regions controlled by activation and diffusion become distinct.

Several papers have been published based on the macroscopic model.[7-10] Paasch *et al.*[7] presented a generalized model for impedance of a macroscopically homogeneous porous electrode under the influence of a potential gradient and the theory was generalized to include an arbitrary time delay of the charge-transfer process at the pore surface. Ong and Newman[8] analyzed a simple representation of the porous electrodes as a resistor-capacitor network. In their paper the expression for the impedance of a porous electrode was derived assuming the concentrations to be constant. Doyle *et al.*[9] simulated the impedance response of a lithium rechargeable battery system numerically including both concentration and potential gradients across the cell. They estimated the solid-phase lithium-ion diffusion coefficient from the impedance spectra in the absence of solution-phase diffusion limitation. Following this, Guo *et al.*[10] investigated the validity of estimating the solid-phase diffusion coefficient of a lithium intercalation electrode from impedance measurements. Guo *et al.* concluded that the validity is not assured if there are mass-transfer limitations in the solution phase. In this paper we analyze the significance of solution-phase diffusional impedance in the porous electrode. Using the macrohomogeneous model and linearization of the current-overpotential relation, we have derived an analytical expression for the impedance response under the influence of both concentration and potential gradients.

The macrohomogeneous model is more useful than the cylindrical pore model because the macrohomogeneous model includes the possibility for current to flow in both the solid and solution phases. Consequently, the performance of a porous electrode can be predicted with the macrohomogeneous model when the conductivities of the solid phase and solution phase are comparable. This may be the case for some intercalation electrodes. For example, the solid-phase conductivity of $Li_{1+x}CoO_2$ is on the order of the conductivity of the electrolyte in the cell studied by Shibuya *et al.*[11] in some cases. Also, the cylindrical pore model has not been used to evaluate the performance of a porous electrode in the cell configuration studied here. Gomadam *et al.*[12] used the macrohomogeneous model to obtain analytical solutions for porous electrodes under three different cell configurations. The geometry of the cell considered here is shown in Fig. 1, which is the same as configuration II of Gomadam *et al.*[12] This cell configuration is useful when the conductivities of the solid phase and solution phase are comparable. The impedance of the setup shown in Fig. 1 could be measured by using a bipotentiostat.

The model presented here can be used to gain physical understanding of the transient behavior of the porous electrode. Using the expression for the impedance, the corresponding ohmic, charge-transfer, and polarization resistances are quantified. The effects of parameters such as exchange current density, porosity, diffusion coefficient, and particle size on the impedance are presented.

Model Development

A schematic diagram of a symmetric porous electrode system is shown in Fig. 1. The porous electrode is described by the macrohomogeneous model,[13] where the inert material, liquid electrolyte, and the active material are considered to be superimposed homogeneous phases. Concentrated solution theory[13] is used to describe the transport in the binary electrolyte (*e.g.*, a mixture of propylene carbonate, dimethyl carbonate, and ethyl methyl carbonate with $LiPF_6$).

The assumptions made in the model are as follows: (*i*) One-dimensional transport. (*ii*) Diffusion coefficient (D), activity coefficient ($f_{\pm}$), transference number (t_+^0), double-layer capacitance (C_{dl}), and porosity (ε) are constants. (*iii*) Solid-phase diffusion is

* Electrochemical Society Student Member.
** Electrochemical Society Active Member.
*** Electrochemical Society Fellow.
z E-mail: white@engr.sc.edu

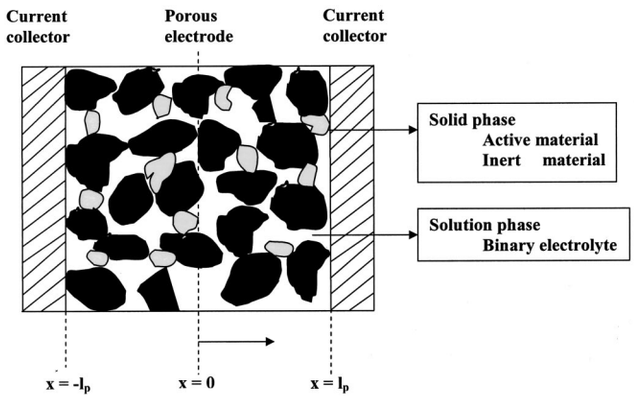

Figure 1. Electrode geometry of a symmetric porous electrode system.

neglected. (*iv*) Separability of the total current density into faradaic and nonfaradaic current densities. (*v*) The interfacial reaction at the solid/liquid interface is a simple charge transfer: Ox + ne^- ⇆ Red. (*vi*) The open-circuit potential (U) is taken to be constant and is set equal to zero. (*vii*) Linear kinetics. (*viii*) Impedance experiments are conducted at open-circuit conditions being zero overpotential and uniform concentration (c_i) across the electrode. (*ix*) When the system is perturbed, change in the value of the exchange current density is invariant with respect to concentration.[14] The material balance in the solution phase taking into account the charge-transfer reaction and charge conservation in the electrode is given by[13]

$$\varepsilon \frac{\partial c}{\partial t} = \varepsilon D_{\text{eff}} \frac{\partial^2 c}{\partial x^2} + a(1 - t_+^0) j_n + \frac{aC_{\text{dl}}(1 - t_+^0)}{F} \frac{\partial(\phi_1 - \phi_2)}{\partial t} \quad [1]$$

where j_n is the pore wall flux of ions across the interface between the electrolyte and the active material and is given by the faradaic current density at the interface represented by the Butler-Volmer equation[13]

$$j_n F = i_0 \left[\exp\left(\frac{\alpha_a F}{RT}\eta\right) - \exp\left(\frac{-\alpha_c F}{RT}\eta\right) \right] \quad [2]$$

The total current density across the solution/pore wall interface is the sum of the faradaic current and the nonfaradaic current. Taking into account the non-faradaic current, which develops from the charging and discharging of the electrochemical double layer at the interface, the conservation of charge leads to the following equation[13]

$$aFj_n = \frac{\partial i_2}{\partial x} - aC_{\text{dl}} \frac{\partial(\phi_1 - \phi_2)}{\partial t} \quad [3]$$

Ohm's law gives the potential in the solid phase[13]

$$i_1 = I - i_2 = -\sigma_{\text{eff}} \frac{\partial \phi_1}{\partial x} \quad [4]$$

where I is the total current density applied. The modified Ohm's law gives the potential in the solution phase[13]

$$i_2 = -\kappa_{\text{eff}} \frac{\partial \phi_2}{\partial x} + \frac{2RT\kappa_{\text{eff}}}{F}(1 - t_+^0) \frac{\partial \ln c}{\partial x} \quad [5]$$

Bruggeman's relation[15,16] is used to determine the effective parameters of the porous electrode from the bulk values

$$D_{\text{eff}} = \varepsilon^{0.5} D \quad [6]$$

$$\kappa_{\text{eff}} = \varepsilon^{1.5} \kappa \quad [7]$$

$$\sigma_{\text{eff}} = (1 - \varepsilon)^{1.5} \sigma \quad [8]$$

The Butler-Volmer equation and the solution phase potential are described by nonlinear equations. Taking advantage of the small perturbations used in EIS, Eq. 2 can be linearized[8] with respect to the overpotential at open-circuit conditions

$$j_n F = \frac{i_0 F(\alpha_a + \alpha_c)\eta}{RT} \quad [9]$$

where $\alpha_a + \alpha_b = n$. Equation 5 can also be linearized with respect to both overpotential and concentration at open-circuit conditions

$$i_2 = -\kappa_{\text{eff}} \frac{\partial \phi_2}{\partial x} + \frac{2RT\kappa_{\text{eff}}}{Fc_i}(1 - t_+^0) \frac{\partial c}{\partial x} \quad [10]$$

Small perturbations correspond to the amplitude of the perturbation smaller than the thermal voltage so that system response is linear.[17] The thermal voltage, V_T, is about 25 mV at 25°C when $n = 1$ according to the definition of the thermal voltage

$$V_T \equiv \frac{RT}{nF} \quad [11]$$

Differentiating Eq. 4 and combining with Eq. 3 gives the governing equation for the solid phase potential

$$\sigma_{\text{eff}} \frac{\partial^2 \phi_1}{\partial x^2} = aFj_n + aC_{\text{dl}} \frac{\partial(\phi_1 - \phi_2)}{\partial t} \quad [12]$$

The governing equation for the solution phase potential is given by combining Eq. 3 and the differential of Eq. 10

$$\kappa_{\text{eff}} \frac{\partial^2 \phi_2}{\partial x^2} = -aFj_n - aC_{\text{dl}} \frac{\partial(\phi_1 - \phi_2)}{\partial t} + \frac{2RT\kappa_{\text{eff}}}{Fc_i}(1 - t_+^0) \frac{\partial^2 c}{\partial x^2} \quad [13]$$

The surface overpotential (η) quantifies the degree to which the system is disturbed from the equilibrium

$$\eta = \phi_1 - \phi_2 - U \quad [14]$$

Because the open-circuit potential (OCP) is set equal to zero, η is given by the potential difference between the solid phase and solution phase

$$\eta = \phi_1 - \phi_2 \quad [15]$$

Based on this definition of the overpotential, the equations for ϕ_1 and ϕ_2 (Eq. 12 and 13) can be combined to write the governing equation for the overpotential

$$\frac{\partial^2 \eta}{\partial x^2} = \left(\frac{1}{\kappa_{\text{eff}}} + \frac{1}{\sigma_{\text{eff}}}\right)\left[aFj_n + aC_{\text{dl}} \frac{\partial \eta}{\partial t}\right] - \frac{2RT}{Fc_i}(1 - t_+^0) \frac{\partial^2 c}{\partial x^2} \quad [16]$$

Substituting for j_n from Eq. 9 into Eq. 1 and 16, we can write the governing equations for the concentration and overpotential as linear second-order partial differential equations

$$\varepsilon \frac{\partial c}{\partial t} = \varepsilon D_{\text{eff}} \frac{\partial^2 c}{\partial x^2} + \frac{ai_0(\alpha_a + \alpha_c)}{RT}(1 - t_+^0)\eta + \frac{aC_{\text{dl}}(1 - t_+^0)}{F} \frac{\partial \eta}{\partial t} \quad [17]$$

$$\frac{\partial^2\eta}{\partial x^2} = \frac{ai_0F(\alpha_a + \alpha_c)}{RT}\left(\frac{1}{\kappa_{eff}} + \frac{1}{\sigma_{eff}}\right)\eta + aC_{dl}\left(\frac{1}{\kappa_{eff}} + \frac{1}{\sigma_{eff}}\right)\frac{\partial\eta}{\partial t} - \frac{2RT(1 - t_+^0)}{Fc_i}\frac{\partial^2 c}{\partial x^2} \quad [18]$$

with the initial conditions for the dependent variables being uniform concentration ($c = c_i$) across the electrode and overpotential equal to zero ($\eta = 0$). The boundary conditions for the porous electrode at $x = -l_p$ are zero concentration flux at

$$x = -1_p \quad \frac{\partial c}{\partial x} = 0 \quad [19]$$

and the current is carried by the solid phase only at

$$x = -l_p \quad \frac{\partial\eta}{\partial x} = -\frac{I}{\sigma_{eff}} \quad [20]$$

The boundary conditions at the other current collector end $x = l_p$ are the same as Eq. 19 and 20. The applied current density (I) is a sinusoidal perturbation of amplitude i_{app} with a frequency 'ω'

$$I(\omega,t) = \mathrm{Re}[i_{app}\exp(j\omega t)] \quad [21]$$

Analytical solution.—Introducing the dimensionless dependent variables

$$c^* = \frac{c - c_i}{c_i} \quad \text{and} \quad \eta^* = \frac{F\eta}{RT} \quad [22]$$

and the dimensionless independent variables

$$X = \frac{x}{l_p} \quad \text{and} \quad \tau = \frac{t}{aC_{dl}\left(\frac{1}{\kappa_{eff}} + \frac{1}{\sigma_{eff}}\right)l_p^2} \quad [23]$$

Equations 17 and 18 can be rewritten in the dimensionless form as follows

$$\frac{\partial^2 c^*}{\partial X^2} = \frac{B_1}{B_2}\frac{\partial c^*}{\partial\tau} - \frac{\nu^2}{B_2}\eta^* - \frac{1}{B_2}\frac{\partial\eta^*}{\partial\tau} \quad [24]$$

$$\frac{\partial^2\eta^*}{\partial X^2} = -2(1 - t_+^0)\frac{B_1}{B_2}\frac{\partial c^*}{\partial\tau} + 2(1 - t_+^0)\left[\frac{\nu^2}{B_2}\eta^* + \frac{1}{B_2}\frac{\partial\eta^*}{\partial\tau}\right] + \nu^2\eta^* + \frac{\partial\eta^*}{\partial\tau} \quad [25]$$

where ν^2, B_1, and B_2 are dimensionless groups defined in Table I.

Taking the Laplace transform of the dimensionless equations yields

$$\frac{\partial^2\overline{c}^*}{\partial X^2} = s\frac{B_1}{B_2}\overline{c}^* - \frac{S}{B_2}\overline{\eta}^* \quad [26]$$

$$\frac{\partial^2\overline{\eta}^*}{\partial X^2} = -s2(1 - t_+^0)\frac{B_1}{B_2}\overline{c}^* + S\frac{2(1 - t_+^0)}{B_2}\overline{\eta}^* + S\overline{\eta}^* \quad [27]$$

where the overbar indicates the dependent variables in the Laplace domain and

$$S = \nu^2 + s \quad [28]$$

The boundary conditions in dimensionless form then become at

Table I. Dimensionless variables.

Dimensionless parameter	Definition
ν^2	$\frac{ai_0Fn}{RT}\left(\frac{1}{\sigma_{eff}} + \frac{1}{\kappa_{eff}}\right)1_p^2$
B_1	$\left(\frac{F^2\varepsilon c_i}{RT(1 - t_+^0)}\right)\frac{1}{aC_{dl}}$
B_2	$\left(\frac{F^2\varepsilon c_i}{RT(1 - t_+^0)}\right)D_{eff}\left(\frac{1}{\kappa_{eff}} + \frac{1}{\sigma_{eff}}\right)$
B_3	$\frac{\nu^2}{B_2}$

$$X = -1 \quad \frac{\partial\overline{c}^*}{\partial X} = 0$$

$$\frac{\partial\overline{\eta}^*}{\partial X} = -\overline{I}^* \quad [29]$$

at

$$X = 1 \quad \frac{\partial\overline{c}^*}{\partial X} = 0$$

$$\frac{\partial\overline{\eta}^*}{\partial X} = -\overline{I}^* \quad [30]$$

where $\overline{I}^*$ is the dimensionless current density in the Laplace domain and the dimensionless current density is defined as

$$I^* = \frac{IFl_p}{RT\sigma_{eff}} \quad [31]$$

Equations 26 and 27 are solved subject to Eq. 29 and 30 using the matrix exponential method as explained in the Appendix.[18] The analytical solutions for the dimensionless concentration and overpotential as functions of the dimensionless distance X, Laplace variables, and the dimensionless groups are

$$\overline{c}^*(X,s) = \frac{(B_2\lambda_2 - B_1s)(B_2\lambda_1 - B_1s)}{2sB_1t_-^0B_2(\lambda_1 - \lambda_2)}\overline{I}^* \times\left[\frac{\sinh(\sqrt{\lambda_2}X)}{\cosh(\sqrt{\lambda_2})\sqrt{\lambda_2}} - \frac{\sinh(\sqrt{\lambda_1}X)}{\cosh(\sqrt{\lambda_1})\sqrt{\lambda_1}}\right] \quad [32]$$

$$\overline{\eta}^*(X,s) = \frac{1}{B_2(\lambda_1 - \lambda_2)}\overline{I}^* \times\left[\frac{(B_2\lambda_2 - B_1s)\sinh(\sqrt{\lambda_2}X)}{\cosh(\sqrt{\lambda_2})\sqrt{\lambda_2}} - \frac{(B_2\lambda_1 - B_1s)\sinh(\sqrt{\lambda_1}X)}{\cosh(\sqrt{\lambda_1})\sqrt{\lambda_1}}\right] \quad [33]$$

where the eigenvalues are given by

$$\lambda_1 = \frac{1}{2B_2}[sB_1 + 2St_-^0 + SB_2 + \sqrt{s^2B_1^2 + 4t_-^0SsB_1 - 2sB_1SB_2 + 4(t_-^0)^2S^2 + 4t_-^0S^2B_2 + S^2B_2^2}]$$

$$\lambda_2 = \frac{1}{2B_2}[sB_1 + 2St_-^0 + SB_2 - \sqrt{s^2B_1^2 + 4t_-^0SsB_1 - 2sB_1SB_2 + 4(t_-^0)^2S^2 + 4t_-^0S^2B_2 + S^2B_2^2}] \quad [34]$$

and

$$t_-^0 = (1 - t_+^0) \quad [35]$$

The perturbed variables in the Laplace domain can be changed to the frequency domain by substituting $j\omega^*$ for s[19] where ω^* is the dimensionless frequency

$$\omega^* = aC_{dl}\left(\frac{1}{\kappa_{eff}} + \frac{1}{\sigma_{eff}}\right)l_p^2\omega \quad [36]$$

Clearly $\overline{c}^*$ and $\overline{\eta}^*$ are complex quantities with real and imaginary parts. Plots of the real and imaginary parts of the variables $\overline{c}^*$ and $\overline{\eta}^*$ at fixed values of low and high dimensionless frequencies ($\omega^* = 6.58 \times 10^{-6}$ and 6.58×10^{1}) are shown in Fig. 2 and 3. For convenience $\overline{I}^*$ is assumed to be equal to one. As shown in Fig. 2 and 3, the perturbed variables (both their real and imaginary parts) do not vary from the steady-state values (zero) at the center of the electrode ($X = 0$). Profiles of the variables for the entire range of dimensionless frequency, $\omega^* = 6.58 \times 10^{-9}$ to 6.58×10^{5} or $\omega = 1\ \mu$Hz to 1 MHz, showed the same trend. Hence, for this particular geometry, one of the boundary conditions can be replaced by the steady-state condition (open-circuit conditions) at the center of the electrode. That is, the boundary conditions can be taken as at

$$X = 0 \quad \overline{c}^* = 0$$
$$\overline{\eta}^* = 0 \quad [37]$$

at

$$X = 1 \quad \frac{\partial \overline{c}^*}{\partial X} = 0$$

$$\frac{\partial \overline{\eta}^*}{\partial X} = -\overline{I}^* \quad [38]$$

The dimensionless concentration and overpotential as functions of position and time solved using the boundary condition given in Eq. 37 and 38 are given by Eq. 32 and 33 divided by two.

Impedance.—In case of impedance measurements, the applied perturbation is a sinusoidal current (Eq. 21). The applied current density introduces a corresponding variation in the potential drop across the porous electrode that is a function of concentration and overpotential. The impedance of the electrode can be determined by the ratio of the potential drop across the porous electrode to the applied current density. The potential drop across the porous electrode is the difference between the solid phase potentials at either end of the electrode. Thus, the dimensionless impedance ($\overline{Z}$) is given by

$$\overline{Z} = \frac{\overline{\phi}_1^*|_{X=-1} - \overline{\phi}_1^*|_{X=1}}{\overline{I}^*} \quad [39]$$

where $\overline{I}^*$ is the dimensionless applied current density (Eq. 31) in the Laplace domain and $\overline{\phi}_1^*$ is the dimensionless perturbed solid-phase potential ($\phi_1^* = \phi_1 F/RT$) in the Laplace domain. In case of the reformulated boundary conditions (Eq. 37 and 38) the impedance is given by

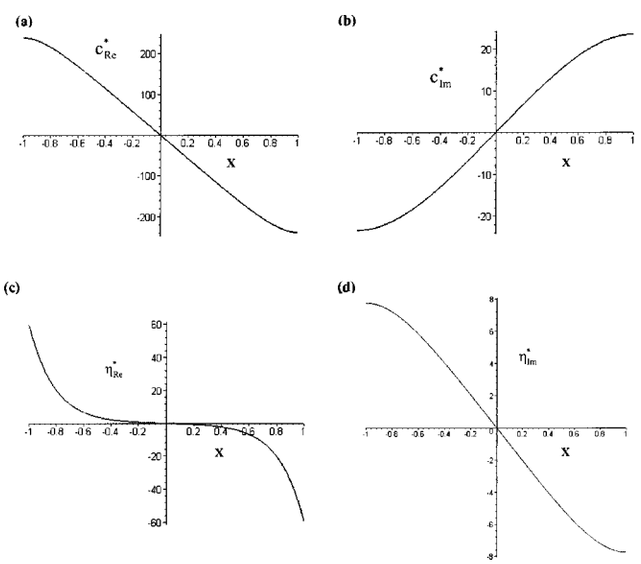

Figure 2. Plot of the perturbed variables along the spatial coordinate and $\omega^* = 6.58 \times 10^{-6}$ (a) c_{Re}^*, (b) c_{Im}^*, (c) η_{Re}^*, and (d) η_{Im}^* (other parameter values given in Table II).

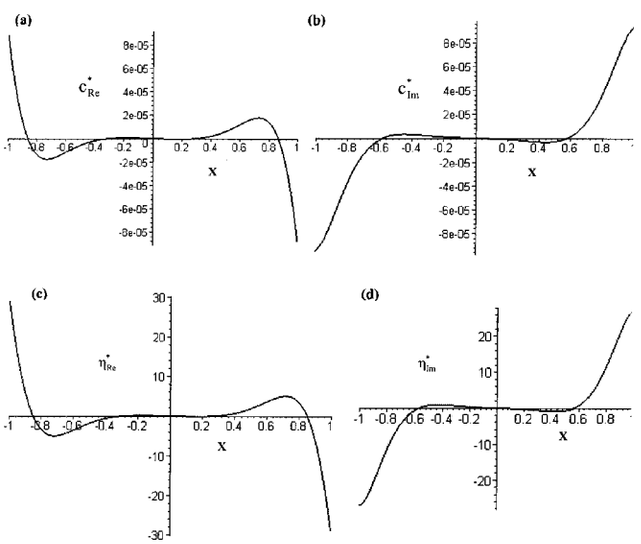

Figure 3. Plot of the perturbed variables along the spatial coordinate and $\omega^* = 6.58 \times 10^{1}$ (a) c_{Re}^*, (b) c_{Im}^*, (c) η_{Re}^*, and (d) η_{Im}^* (other parameter values given in Table II).

$$\overline{Z} = \frac{2(\overline{\phi}_1^*|_{X=0} - \overline{\phi}_1^*|_{X=1})}{\overline{I}^*} \quad [40]$$

Dimensionless solid-phase potential drop across the electrode is a function of the dimensionless overpotential and concentration. Substituting Eq. 12 into 18 and introducing the dimensionless variables given in Eq. 22, 23, and $\overline{\phi}_1^*$, the governing equation for the solid-phase potential in terms of the dimensionless overpotential and concentration is determined as

$$\frac{\partial^2\overline{\phi}_1^*}{\partial X^2} = \frac{1}{(\beta + 1)}\frac{\partial^2\overline{\eta}^*}{\partial X^2} + \frac{2t_-^0}{(\beta + 1)}\frac{\partial^2\overline{c}^*}{\partial X^2} \quad [41]$$

where

$$\beta = \frac{\sigma_{\text{eff}}}{\kappa_{\text{eff}}}$$

Integration of Eq. 41 with respect to X gives the dimensionless solid-phase potential in terms of the integration constant (A)

$$\frac{\partial\overline{\phi}_1^*}{\partial X} = \frac{1}{(\beta + 1)}\frac{\partial\overline{\eta}^*}{\partial X} + \frac{2t_-^0}{(\beta + 1)}\frac{\partial\overline{c}^*}{\partial X} + A \quad [42]$$

The integration constant can be determined from the boundary conditions at

$$X = 1 \quad \frac{\partial\overline{x}^*}{\partial X} = \frac{\partial\overline{\phi}_1^*}{\partial X} = -\overline{I}^* \quad [43]$$

and at

$$X = 1 \quad \frac{\partial\overline{c}^*}{\partial X} = 0 \quad [44]$$

as

$$A = \frac{-\beta\overline{I}^*}{(\beta + 1)} \quad [45]$$

Further, integrating Eq. 42 with respect to X from 0 to 1 and substituting for A gives the dimensionless solid-phase potential drop across the porous electrode

$$(\overline{\phi}_1^*|_{X=0} - \overline{\phi}_1^*|_{X=1}) = \frac{-\kappa_{\text{eff}}}{\kappa_{\text{eff}} + \sigma_{\text{eff}}}[\overline{\eta}^*|_{X=1} + 2(1 - t_+^0)\overline{c}^*|_{X=1}] + \frac{\sigma_{\text{eff}}}{\kappa_{\text{eff}} + \sigma_{\text{eff}}}\overline{I}^* \quad [46]$$

where the dimensionless overpotential and concentration at $X = 1$ can be evaluated using the expressions given in Eq. 32 and 33, respectively. Hence, the final expression for the dimensionless impedance in the Laplace domain ($\overline{Z}$) evaluated using Eq. 40 can be transformed to the dimensionless impedance in the frequency domain (Z) by replacing s with $j\omega^*$,[19] written as

$$Z = \frac{2\kappa_{\text{eff}}}{(\sigma_{\text{eff}} + \kappa_{\text{eff}})(\lambda_1 - \lambda_2)sB_1}\left[\frac{\lambda_2(\lambda_1 B_2 - sB_1)\tanh(\sqrt{\lambda_1})}{\sqrt{\lambda_1}} - \frac{\lambda_1(\lambda_2 B_2 - sB_1)\tanh(\sqrt{\lambda_2})}{\sqrt{\lambda_2}}\right] + \frac{2}{\left(1 + \frac{\kappa_{\text{eff}}}{\sigma_{\text{eff}}}\right)} \quad [47]$$

where

$$s = j\omega^* \quad [48]$$

Table II. Parameter values.

Parameter	Value	Ref.
i_0	0.00018 A/cm^2	Ong and Newman[8]
κ	4.11×10^{-4} S/cm	Ong and Newman[8]
σ	0.003 S/cm	[a]
l_p	0.008 cm	[a]
D	7.5×10^{-9} cm^2/s	[a]
ε	0.53	[a]
$\varepsilon_{\text{inert}}$	0.073	Ong and Newman[8]
R_s	8.5 μm	Ong and Newman[8]
a	1401.2 cm^{-1}	Calculated using Eq. 57
C_{dl}	10 μF/cm^2	Ong and Newman[8]
$\alpha_a + \alpha_c$	n	Newman
n	1	[a]
c_i	0.001 mol/cm^3	Ong and Newman[8]
t_+^0	0.537	Ong and Newman[8]
ν^2	4.612	[b]
B_1	3.06827×10^5	[b]
B_2	0.1723	[b]
B_3	26.77	[b]

[a] Assumed value.
[b] Calculated using the definition in Table I.

The dimensionless impedance in the frequency domain is a complex number with real part (Z_{Re}) and imaginary part ($Z_{i\mathbf{m}}$). The expressions for the real and imaginary part are too long to be presented here. They can be obtained using the standard commands in maple.[20] Maple programs used in this paper can be obtained upon request (White).

Results and Discussion

The impedance was simulated for the $Li_yMn_2O_4$ electrodes using the base values given in Table II and the derived analytical solution. The impedance spectrum for the $Li_yMn_2O_4$ electrodes was also solved numerically using the method employed by Doyle *et al.*[9] The results obtained from the analytical solution agree well with those from the numerical solution. The impedance spectrum, illustrated in Fig. 4, shows two well-defined arcs with a very high-frequency intercept.

The higher frequency arc represents the kinetic impedance and the lower frequency arc represents the diffusional impedance. The kinetic arc is a squashed semicircle due to the linear impedance behavior (slope equal to 45°, as shown by the inset in Fig. 4) at very high frequencies, while the diffusional impedance is a perfect semicircle. The 45° straight line, typical of porous electrodes, is due to the distributed interfacial impedance that is purely capacitive at very high frequencies.[1,5,14] When the system is perturbed from the equilibrium condition (open-circuit condition) electrode kinetics is the

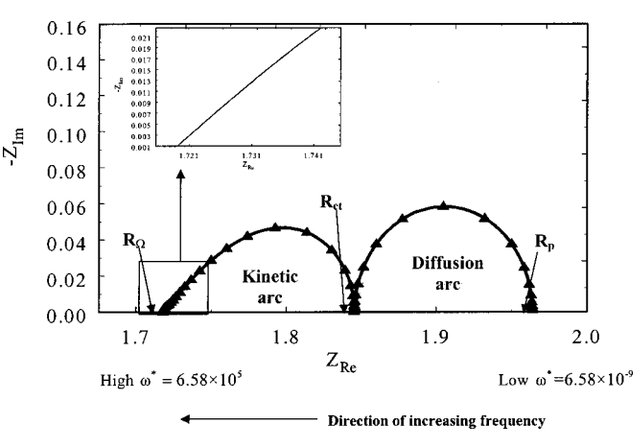

Figure 4. Impedance response for $Li_yMn_2O_4$ electrodes (parameter values are given in Table II): (——) analytical and (▲) numerical solution.

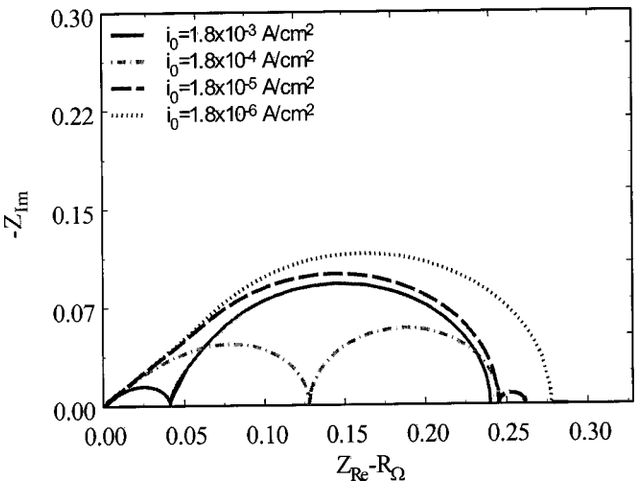

Figure 5. Effect of exchange current density on the impedance response (other parameter values given in Table II).

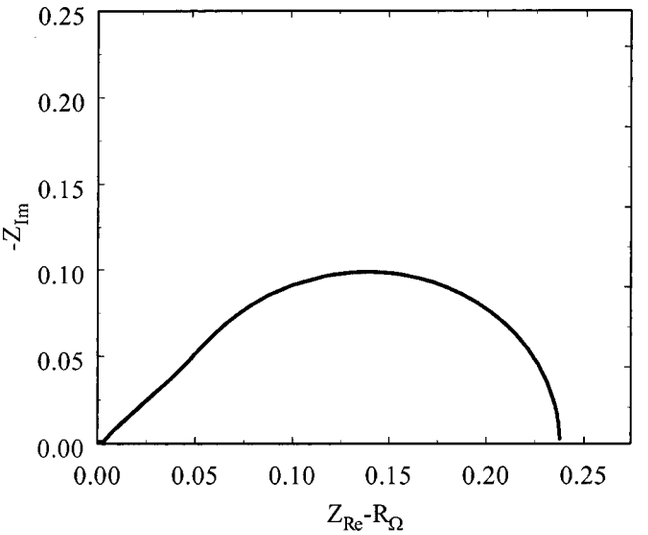

Figure 6. Diffusion-limited impedance spectrum (i_0 = 0.048 A/cm^2, other parameter values given in Table II).

main cause for a change in the electrode potential. However, in the presence of the double-layer capacitance at the interface, the charging and discharging of the double layer acts as a parallel phenomenon in establishing the potential gradients. This translates into the kinetic arc in the high-frequency regime. In the low-frequency regime, the electrode reaction is fast, but the rate of the diffusion process is not fast enough to supply the reacting species. This leads to concentration gradients in the solution phase giving rise to mass-transfer resistance. The impedance spectra shown here are similar to the results obtained by Cachet and Wiart[4] and Lasia.[5] They used a cylindrical pore model and numerical methods to solve for the impedance of a porous electrode under the influence of potential and concentration gradients.

At very high frequencies the double-layer capacitance short-circuits the surface overpotential, leaving the ohmic drop across the solid matrix and the solution phase as the residual resistance. The dimensionless ohmic resistance (R_Ω)[3,12] is the high-frequency intercept that can be evaluated from the impedance expression (Eq. 47 after substitution of Eq. 48) for $\omega^* \to \infty$ yielding

$$Z \to R_\Omega = \frac{2}{\left(1 + \frac{\kappa_{eff}}{\sigma_{eff}}\right)} = 1.718132 \qquad [49]$$

using the values given in Table II.

A plot of the impedance spectra for different values of the exchange current density is shown in Fig. 5. Note that the dimensionless ohmic resistance (R_Ω) of the electrode was deducted from the real part of the impedance spectra in Fig. 5 for better representation of the impedance arcs. The same format is followed for Fig. 6-10. Exchange current density, expressed as the product of rate constant and local concentrations in the solid and solution phase,[15] can be seen as the electrochemical reaction rate. At moderate reaction rates, both the diffusional impedance and the kinetic impedance contribute to the total impedance across the porous electrode, as indicated by two arcs. At low values of the exchange current density, though flux of the species is maintained high by the diffusion process the kinetics at the interface is slow and offers maximum resistance, leading to an impedance spectrum with a large kinetic arc and no diffusional arc. The performance of the porous electrode in this case is limited by the interfacial kinetics, and the impedance expression in Eq. 47 is reduced to

$$Z = 2\frac{\kappa_{eff}}{(\kappa_{eff} + \sigma_{eff})}\frac{\tanh(\sqrt{s + \nu^2})}{\sqrt{s + \nu^2}} + 2\frac{\sigma_{eff}}{(\kappa_{eff} + \sigma_{eff})} \qquad [50]$$

where $s = j\omega^*$. Equation 50 gives the dimensionless impedance for the symmetric system of porous electrodes when the potential drop governs the impedance. Equation 50 is the same as the impedance expression derived by Gomadam *et al.*[12] for the porous electrodes with no concentration gradients. The low-frequency intercept of the kinetic arc in this case is the charge transfer (R_{ct}),[3,4,21] obtained by taking the limit $\omega^* \to 0$ in Eq. 50, giving

$$R_{ct} = 2\frac{\kappa_{eff}}{(\kappa_{eff} + \sigma_{eff})}\frac{\tanh(\nu)}{\nu} + 2\frac{\sigma_{eff}}{(\kappa_{eff} + \sigma_{eff})} \qquad [51]$$

Let us consider the case when the kinetics at the interface is fast. Here, in spite of the higher rate of reaction the total impedance of the electrode is high. This is because the diffusion process is not fast enough to supply enough reactant to maintain the interfacial reaction at such high rates. The diffusional impedance dominates the porous electrode, indicated by a larger diffusion arc when compared to the kinetic arc. In Fig. 5 the impedance arc for higher values of the exchange current density indicates that the total impedance is not completely governed by the diffusion process; there exists a small kinetic resistance also. When the exchange current density is increased to further higher values the impedance in the porous electrode is completely dominated by the diffusion resistance, as shown in Fig. 6. In this case the performance of the porous electrode is diffusion limited. The impedance spectra of the diffusion-limited process also exhibits a linear behavior at high frequencies similar to the kinetic arc due to the porous nature of the electrodes. The low-frequency intercept of the diffusional arc ($\omega^* \to 0$) gives the polarization resistance (R_p)[3,4]

$$R_p = \frac{2}{1 + \frac{\kappa_{eff}}{\sigma_{eff}}} + 2\frac{\kappa_{eff}}{\kappa_{eff} + \sigma_{eff}}\left[\frac{2t^0}{(2t^0 + B_2)} + \frac{B_2}{(2t^0 + B_2)}\frac{\tanh\left(\sqrt{\frac{\nu^2}{B_2}(2t^0 + B_2)}\right)}{\sqrt{\frac{\nu^2}{B_2}(2t^0 + B_2)}}\right] \qquad [52]$$

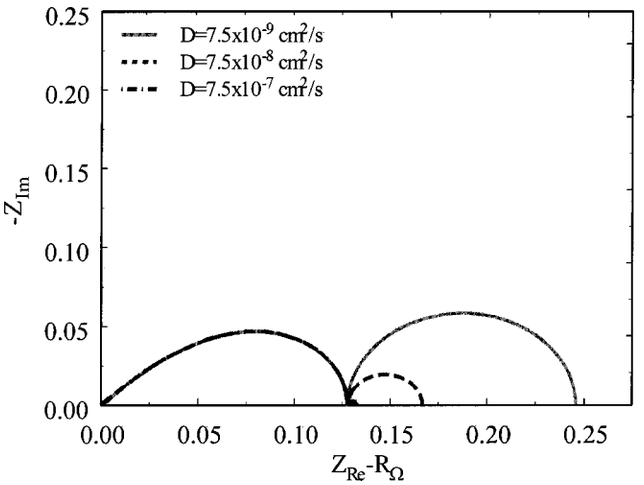

Figure 7. Effect of bulk diffusion coefficient on the impedance response (other parameter values given in Table II).

The diffusion coefficient of the species involved is an important property that determines the concentration gradient in the porous electrode. Figure 7 gives the impedance spectra for different values of the solution-phase diffusion coefficient. The value of the diffusion coefficient does not affect the kinetic semicircle. A larger diffusional arc is obtained for low values of the bulk diffusion coefficient of about $D = 7.5 \times 10^{-9}$ cm^2/s. This shows that significant concentration gradients are established in the case of electrolytes in which the diffusion coefficient of the species is low like the polymer electrolytes. The dimensionless group B_3 determines the importance of concentration gradients and the potential gradients in the porous electrode, given by

$$B_3 = \frac{\nu^2}{B_2} = \frac{i_0}{F}\frac{an(1 - t_+^0)}{\varepsilon c_i}\left(\frac{l_p^2}{D_e}\right) \qquad [53]$$

or

$$B_3 = \frac{\text{kinetic flux}}{\text{diffusion flux}} \qquad [54]$$

where

$$\text{kinetic flux} = \frac{ni_0(1 - t_+^0)}{F} \qquad [55]$$

and

$$\text{diffusion flux} = \varepsilon c_i\left(\frac{D_e}{l_p^2}\right) \qquad [56]$$

Case 1: Kinetic limited impedance.—When the flux ratio becomes much smaller than one, $B_3 \ll 1$, kinetics are more important and the impedance spectrum obtained is only the kinetic arc (see Fig. 5 for $i_0 = 1.8 \times 10^{-6}$ A/cm^2).

Case 2: Diffusion-limited impedance.—The impedance of the electrode is diffusion limited when the kinetic flux ratio is far greater than the diffusion flux $B_3 \gg 1$ (see Fig. 6).

Similar to the previous analysis, Lasia[5,21] analyzed the effect of concentration gradients based on the value of the parameter $B = (2k_s l^2/rD)p^{-\alpha}(1 + p)$ or $\nu = nFDc_0^*$, where k_s is the standard rate constant, D is the diffusion coefficient, c_0^* is the concentration of the oxidized forms outside the pore, and $p = e^{nF/RT\eta}$. He stated that when $B \to 0$ or $\nu \ll 0$ the electrochemical process in the pores is determined by the concentration gradient only. When $B \to \infty$ or $\nu \gg 0$, the concentration gradient is negligible.

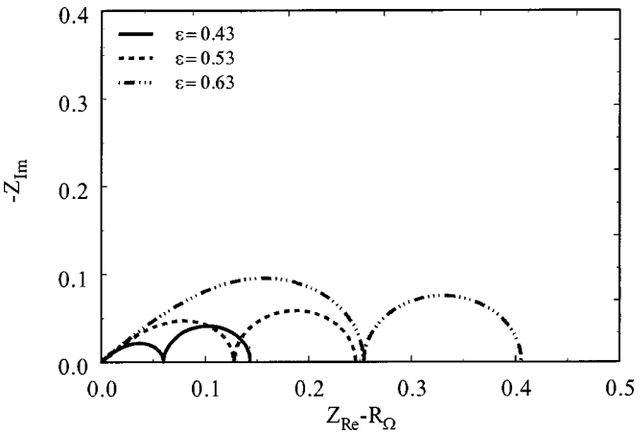

Figure 8. Effect of porosity of the active material on the impedance response (other parameter values given in Table II).

The flux ratio as given in Eq. 54 depends on the properties of the porous electrode and electrolyte. These properties include exchange current density, diffusion coefficient, porosity, thickness of the electrode, and the specific surface area. The specific surface area (a) for the model presented here is defined as the electroactive surface area of the pore walls per unit volume of the total electrode. For spherical particles the specific surface area is related to the particle radius (R_s), porosity of the electrode (ε), and the volume fraction of the inert material (ε_{inert}) as[10]

$$a = \frac{3}{R_s}(1 - \varepsilon - \varepsilon_{inert}) \qquad [57]$$

A change in the interfacial area (a) can be affected by changing the particle size, porosity of the electrode, or the volume fraction of the inert material. Figures 8 and 9 present the influence of these parameters on the impedance spectra. The interfacial area increases with decrease in porosity or particle size. Porosity also affects the ohmic drop across the electrode. This is because the conductivity of the electrolyte and the solid matrix are expressed in terms of effective parameters that depend on the volume fraction of the respective phases. With a decrease in porosity the ohmic drop across the elec-

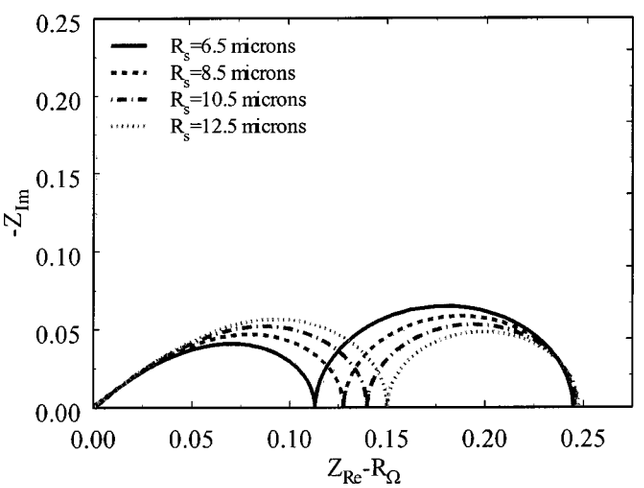

Figure 9. Effect of radius of the active material particles on the impedance response (other parameter values given in Table II).

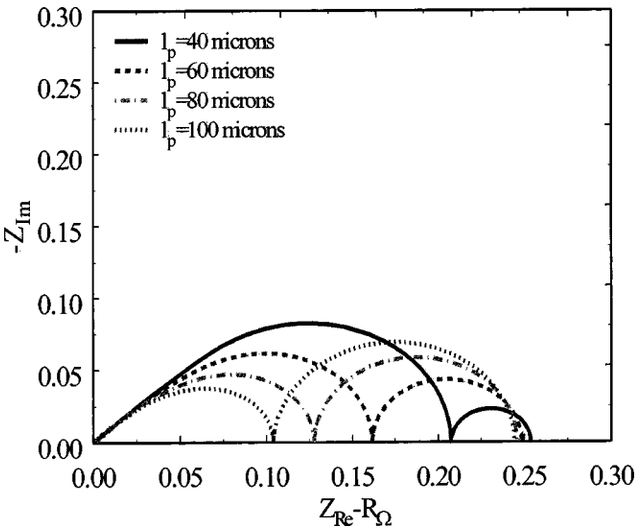

Figure 10. Effect of half the thickness of the porous electrode on the impedance response (other parameter values given in Table II).

trode increases. The effect of l_p on the impedance spectrum is shown in Fig. 10. As the electrode thickness is increased, Eq. 53 and 54 show that the kinetic flux increases relative to the diffusional flux, which is to be expected. A lower diffusion flux gives rise to higher diffusional resistance. This manifests as a smaller kinetic arc and a larger diffusional arc in the impedance spectra of Fig. 10.

Conclusion

An analytical solution for the impedance of a porous electrode with concentration and potential gradients was derived (see Eq. 47). The effect of parameters on the impedance response was studied. Based on the value of B_3 (see Table I) the significance of the solution-phase concentration gradients were analyzed. Concentration gradients become significant at very high exchange current densities as in cells operating at high temperatures and very low diffusion coefficients as in the case of a few polymer electrolytes, when the solid-phase diffusion does not limit the process (small particle size).

Acknowledgments

The authors gratefully acknowledge financial support from the National Reconnaissance Office (NRO) under contract no. 000-03-C-0122.

The University of South Carolina assisted in meeting the publication costs of this article.

Appendix

The coupled linear differential equations in Eq. 26 and 27 can be decoupled and solved analytically by using a similarity matrix transformation method as described here. The second-order differential equations (Eq. 26 and Eq. 27) can be rewritten in the matrix form as follows

$$\frac{d^2Y}{dX^2} = AY \qquad [A\text{-}1]$$

where

$$Y = \begin{bmatrix} y_1 \\ y_2 \end{bmatrix} = \begin{bmatrix} \overline{c}^* \\ \overline{\eta}^* \end{bmatrix} \qquad [A\text{-}2]$$

and

$$\frac{d^2Y}{dX^2} = \begin{bmatrix} \frac{d^2y_1}{dX^2} \\ \frac{d^2y_2}{dX^2} \end{bmatrix} = \begin{bmatrix} \frac{d^2\overline{c}^*}{dX^2} \\ \frac{d^2\overline{\eta}^*}{dX^2} \end{bmatrix} \qquad [A\text{-}3]$$

$$A = \begin{bmatrix} \frac{sB_1}{B_2} & -\frac{S}{B_2} \\ -\frac{2s(1-t_+^0)B_1}{B_2} & S\left(\frac{2(1-t_+^0)}{B_2} + 1\right) \end{bmatrix} \qquad [A\text{-}4]$$

The matrix equation (Eq. A-1) can be transformed into Eq. A-5 using the matrix of eigenvectors (**P**)

$$\frac{d^2(\mathbf{M})}{dx^2} = \gamma\mathbf{M} \qquad [A\text{-}5]$$

$$\mathbf{M} = \mathbf{P}^{-1}Y \qquad [A\text{-}6]$$

$$\gamma = \mathbf{P}^{-1}\mathbf{A}\mathbf{P} \qquad [A\text{-}7]$$

where the matrix of eigenvectors **P** expressed in terms of the eigenvalues (λ_1 and λ_2)

$$\mathbf{P} = \begin{bmatrix} \frac{\lambda_2 B_2 - sB_1}{2sB_1(1-t_+^0)} & \frac{\lambda_1 B_2 - sB_1}{2sB_1(1-t_+^0)} \\ 1 & 1 \end{bmatrix} \qquad [A\text{-}8]$$

and γ is a diagonal matrix with the eigenvalues as the elements

$$\gamma = \begin{bmatrix} \lambda_1 & 0 \\ 0 & \lambda_2 \end{bmatrix} \qquad [A\text{-}9]$$

The matrix equation (Eq. A-5) can be decoupled using the eigenvalues of **A** vector as

$$\frac{d^2M_1}{dX^2} = \lambda_1 M_1 \qquad [A\text{-}10]$$

and

$$\frac{d^2M_2}{dX^2} = \lambda_2 M_2 \qquad [A\text{-}11]$$

where M_1 and M_2 are the elements of the vector **M**.

$$\mathbf{M} = \begin{bmatrix} M_1 \\ M_2 \end{bmatrix} \qquad [A\text{-}12]$$

The second-order differential Eq. A-10 and A-11 can be solved for the vector **M** in terms of unknown constants α, α_2, β, and β_2

$$M_1 = \frac{\alpha \sinh(\sqrt{\lambda_1}X)}{\sqrt{\lambda_1}} + \frac{\alpha_2 \cosh(\sqrt{\lambda_1}X)}{\sqrt{\lambda_1}} \qquad [A\text{-}13]$$

$$M_2 = \frac{\beta \sinh(\sqrt{\lambda_2}X)}{\sqrt{\lambda_2}} + \frac{\beta_2 \cosh(\sqrt{\lambda_2}X)}{\sqrt{\lambda_2}} \qquad [A\text{-}14]$$

The perturbed variables $\overline{c}^*$ and $\overline{\eta}^*$ can be determined by premultiplying matrix **M** by the matrix of eigenvectors **P** (from Eq. A-5). The solution for the perturbed variables is in terms of the unknown constants. The constants are determined using the boundary conditions in the dimensionless form as given by the following equations at

$$X = -1 \quad \frac{\partial\overline{c}^*}{\partial X} = 0$$

$$\frac{\partial\overline{\eta}^*}{\partial X} = -\overline{I}^* \qquad [A\text{-}15]$$

at

$$X = 1 \quad \frac{\partial\overline{c}^*}{\partial X} = 0$$

$$\frac{\partial\overline{\eta}^*}{\partial X} = -\overline{I}^* \qquad [A\text{-}16]$$

The constants are determined to be

$$\alpha_2 = \beta_2 = 0 \qquad [A\text{-}17]$$

$$\alpha = \frac{-\overline{I}^*(\lambda_1 B_2 - sB_1)}{B_2(\lambda_1 - \lambda_2)\cosh(\sqrt{\lambda_1})} \qquad [A\text{-}18]$$

$$\beta = \frac{\overline{I}^*(\lambda_2 B_2 - sB_1)}{B_2(\lambda_1 - \lambda_2)\cosh(\sqrt{\lambda_2})} \qquad [A\text{-}19]$$

Using the expressions for the constants as determined here, the dimensionless concentration and overpotential ($\overline{c}^*$ and $\overline{\eta}^*$) are determined as given in Eq. 32 and 33 of the main section.

List of Symbols

a	specific interfacial area, cm^{-1}
B_1	dimensionless group, see Table I
B_2	dimensionless group, see Table I
B_3	dimensionless group, see Table I
c	concentration of lithium ions in the solution phase, mol/cm^3
c_i	concentration of lithium ions in the solution phase at open-circuit conditions, mol/cm^3
c^*	dimensionless concentration, $c - c_i/c_i$
$\overline{c}^*$	dimensionless concentration in the Laplace domain (see Eq. 32)
c^*_{Re}	real part of dimensionless concentration
c^*_{Im}	imaginary part of dimensionless concentration
C_{dl}	double-layer capacitance, $Farad/cm^2$
D	bulk solution salt diffusion coefficient, cm^2/s
D_{eff}	effective diffusivity, cm^2/s (see Eq. 6)
e	charge on the electron, 1.602×10^{-19} C
F	Faraday's constant, 96,487 C/equiv
$f_\pm$	activity coefficient of the salt
I	total current density applied to the system, A/cm^2 (see Eq. 21)
I^*	dimensionless applied current in Laplace domain density, $IFl_p/RT\sigma_{eff}$
$\overline{I}^*$	dimensionless applied current density in the Laplace domain
i_0	exchange current density, A/cm^2
i_1	matrix phase current density, A/cm^2
i_2	solution phase current density, A/cm^2
i_{app}	amplitude of the applied sinusoidal current, A/cm^2
j_n	pore wall flux across interface, $mol/cm^2/s$
k	Boltzman constant, 1.38×10^{-23} J/K
l_p	half the thickness of the porous electrode, cm
n	number of electrons transferred in the electrochemical reaction ($n = 1$ here)
R	universal gas constant, 8.313 J/mol K
R_{ct}	dimensionless charge-transfer resistance (see Eq. 51)
R_p	dimensionless poralization resistance (see Eq. 52)
R_s	radius of the particle, cm
R_Ω	dimensionless ohmic resistance (see Eq. 49)
S	dimensionless variable (see Eq. 28)
s	Laplace variable
T	temperature, K
t	time, s
t^0_+	transference number of lithium ions in the solution
U	open-circuit potential, V
X	dimensionless spatial coordinate, x/l_p
x	distance from the center of the electrode, cm
$\overline{Z}$	dimensionless impedance in the Laplace domain
Z	dimensionless impedance in the frequency domain (see Eq. 47)
Z_{Re}	real part of the dimensionless impedance
Z_{Im}	imaginary part of the dimensionless impedance

Greek

α_a	anodic transfer coefficient, dimensionless
α_c	cathodic transfer coefficient, dimensionless
ε	porosity of the electrode, dimensionless
ε_{inert}	volume fraction of the inert material of the porous electrode
ϕ_1	solid-phase potential, V
ϕ_1^*	dimensionless solid-phase potential, $\phi_1 F/RT$
$\overline{\phi}_1^*$	dimensionless solid-phase potential in the Laplace domain
ϕ_2	solution-phase potential, V
η	surface overpotential, V
η^*	dimensionless overpotential, $(\phi_1\text{-}\phi_2)F/RT$
$\overline{\eta}^*$	dimensionless overpotential in the Laplace domain (see Eq. 33)
η^*_{Re}	real part of the dimensionless overpotential
η^*_{Im}	imaginary part of the dimensionless overpotential
κ	conductivity of bulk solution, S/cm
κ_{eff}	effective solution-phase conductivity, S/cm (see Eq. 7)
ν^2	dimensionless exchange current density (see Table I)
ν	square root of the dimensionless exchange current density
σ	conductivity of the solid phase in the electrode, S/cm
σ_{eff}	effective solid-phase conductivity, S/cm (see Eq. 8)
τ	dimensionless time, $t/aC_{dl}(1/\kappa_{eff} + 1/\sigma_{eff})l_p^2$
ω	frequency, s^{-1}
ω^*	dimensionless frequency, $(aC_{dl}(1/\kappa_{eff} + 1/\sigma_{eff})l_p^2)\omega$

Subscripts

a	anodic
c	cathodic
eff	effective
1	solid phase
2	solution phase

Superscripts

*	dimensionless quantities
overbar	Laplace domain

References

1. R. de Levie, *Advances in Electrochemistry and Electrochemical Engineering*, P. Delahay, Editor, Vol. 6, p. 329, Interscience Publishers, New York (1967).
2. A. Lasia, *J. Electroanal. Chem.*, **397**, 27 (1995).
3. M. Keddam, C. Rakotomavo, and H. Takenouti, *J. Appl. Electrochem.*, **14**, 437 (1984).
4. C. Cachet and R. Wiart, *J. Electroanal. Chem. Interfacial Electrochem.*, **195**, 21 (1985).
5. A. Lasia, *J. Electroanal. Chem.*, **428**, 155 (1997).
6. S. K. Rangarajan, *J. Electroanal. Chem. Interfacial Electrochem.*, **22**, 89 (1969).
7. G. Paasch, K. Micka, and P. Gersdorf, *Electrochim. Acta*, **38**, 2653 (1993).
8. I. J. Ong and J. Newman, *J. Electrochem. Soc.*, **146**, 4360 (1999).
9. M. Doyle, J. P. Meyers, and J. Newman, *J. Electrochem. Soc.*, **147**, 99 (2000).
10. Q. Guo, V. R. Subramanian, J. W. Weidner, and R. E. White, *J. Electrochem. Soc.*, **149**, A307 (2002).
11. M. Shibuya, T. Nishina, T. Matsue, and I. Uchida, *J. Electrochem. Soc.*, **143**, 3157 (1996).
12. P. M. Gomadam, J. W. Weidner, T. A. Zawodzinski, and A. P. Saab, *J. Electrochem. Soc.*, **150**, E371 (2003).
13. J. S. Newman, *Electrochemical Systems*, 2nd ed., Prentice Hall, Englewood Cliffs, NJ (1991).
14. J. P. Meyers, M. Doyle, R. M. Darling, and J. Newman, *J. Electrochem. Soc.*, **147**, 2930 (2000).
15. P. M. Gomadam, J. W. Weidner, R. A. Dougal, and R. E. White, *J. Power Sources*, **110**, 267 (2002).
16. P. De Vidts and R. E. White, *J. Electrochem. Soc.*, **144**, 1343 (1997).
17. J. R. Macdonald, *Impedance Spectroscopy*, Emphasizing Solid Materials and Systems, John Wiley and Sons, Inc., New York (1987).
18. V. R. Subramanian and R. E. White, *Chem. Eng. Educ.*, **34**, 328 (2000).
19. A. Lasia, *Modern Aspects of Electrochemistry*, No. 32, B. E. Conway, J. O'M. Bockris, and R. E. White, Editors, Plenum Publishers, New York (1999).
20. S. Devan, M.S. Thesis, University of South Carolina, Columbia, SC (2003).
21. A. Lasia, *J. Electroanal. Chem.*, **500**, 30 (2001).